2012

Coarse-grained molecular dynamics simulation of a single polymer chain in shear flows

Wei Wei
Lehigh University

Coarse-grained molecular dynamics simulation of a single polymer chain in shear flows

by

Wei Wei

A Thesis

Presented to the Graduate and Research Committee

of Lehigh University

in Candidacy for the Degree of

Master of Science

in

Mechanical Engineering

Lehigh University

August 2012

Thesis is accepted and approved in partial fulfillment of the requirements for the Master of Science in Mechanical Engineering.

Coarse-grained molecular dynamics simulation of a single polymer chain in shear flow
Wei Wei

_____

Date Approved

_____

Thesis Advisor

_____

(Name of Department Chair)

ACKNOWLEDGMENTS

I would like to thank my advisor, Dr. Alparslan Oztekin, for his guidance and support throughout the production of this research and thesis. I would also like to thank Dr. Xiaohui Zhang and Dr. Edmund Webb III, for helpful suggests and encouragement.

Thanks to my friend Haolin Ma for his help on FORTRAN coding. I would also like to thank all my colleagues and friends at Lehigh University, for their unwavering support and encouragement throughout the years.

TABLE OF CONTENTS

LIST OF FIGURES

ABSTRACT

In this study, Brownian dynamics simulations of a single polymer chains are performed. The polymer chain is modeled by a sequence of beads connected by finitely extensible non-linear elastic springs. Coarse-grained molecular dynamic simulations are conducted to investigate flow induced conformational changes of a single polymer chain in a simple shear flow. The present model includes Brownian dynamic force, FENE spring force, Lennard-Jones potential for bead-bead and spring-spring interaction and hydrodynamic interaction of beads with flowing solvent. Different cases are simulated by using different combination of interactions; spring force and Brownian dynamic force are throughout included. Simulations are performed for various shear flow conditions. In some cases, springs are forced to be uncrossable, a soft potential is used to account for the repulsive force between springs. The dependence of bead radius and the coil size of the chain have been tested. Full hydrodynamic interaction is applied along with spring force, Brownian dynamic force and Lennard-Jones potential. Spring-spring repulsion helps the unfolding process, while HI impedes this process. As the intensity of shearing increases, the extension of unfolding increases.

Chapter 1. Introduction

In human bodies, bleeding is stopped by forming a clot at the site of vascular damage. Critical steps in the process are the accumulation and aggregation of platelets at the damaged vessel wall, forming so called platelet "plugs" [1]. Under rapid flow condition such as in arteries and arterioles, however, platelets cannot adhere themselves to vessel wall due to the strong hydrodynamic force imposed by the flowing fluid. In such scenarios the plasma protein von Willebrand Factor (vWF) plays an indispensable role in sticking to both platelets and vessel wall, allowing the formation of platelet plugs [2] [3]. Research shows that DNA molecules such as vWF act as a flow sensor, responding to strong hydrodynamic forces by changing its conformation [4]. In 1990s, Perkins and co-workers stretched single DNA molecules by a flow [5]. The fluctuating chain was imaged have a cone-like envelope and shows a sharp increase in intensity at the free end. Similar phenomenon has been observed that vWF changes conformation under a certain shear rate, becoming unfolded. However, the exact mechanism of how vWF senses flow by presumably switching between the two conformations is still exclusive.

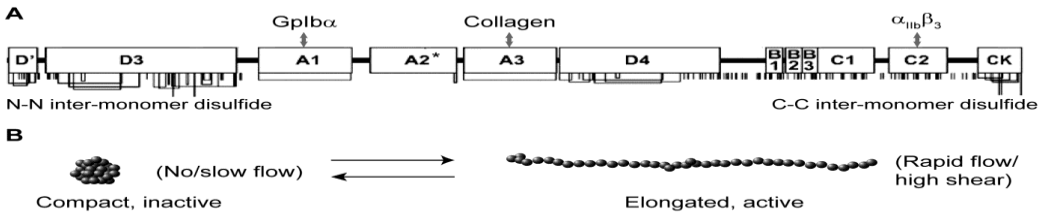

Figure 1(a) Schematic illustration of vWF's domain arrangement. Cysteines are shown as vertical lines and are connected for chemically defined disulfides. Each monomer contains 12 domains. Domains interacting with Gplbα, $\alpha_{11b}\beta_3$ (both on platelets) and collagen (on damaged vessel wall) are indicated by double-sided arrows. A2domin

(indicated by asterisk) unfolds when it is subject to pulling forces. (b) Possible mechanism of flow-induced conformational change. vWF is a long multimer containing up to 200 monomers. Each monomer is modeled as sphere. (X. Zhang 2011)

The overall goal of this study is to use molecular dynamics simulation to study the mechanism of flow induced conformational change in biopolymers. Theoretical modeling will be conducted to attain a clear picture of how vWF molecules achieve flow sensing at the single polymer level.

As is well known, the Gaussian chain model is the simplest model for polymer simulation, which allows an indefinite extension when increasing shear rate or other force. Freely-jointed chain (FJC), introduced by Peterlin in 1966, is the modification of Gaussian model [6]. The real chain is replaced by a set of points connected by rigid robs of fixed length. Kratky and Porod modified the Gaussian model of the worm-like chain (WLC) [7]. In this model, beads are connected by flexible, inextensible robs, which have fixed length. Worm-like chain is more complicated, but it is better than freely-jointed chain when describing helical structures. Bead-Spring chain model replace robs in FJC and WLC by completely flexible springs, also called "Rouse model" [8]. This model is the simplest idealization of a polymer molecule that captures the essential physics required to simulate polymer dynamics. One main limitation of this model is that Hydrodynamic interaction (HI) is neglected. It has been reported that HI plays an important role in polymer dynamics. Bird perfected this model by including Hydrodynamic interaction in 1987 [4]. Katz further examined the behavior of a single polymer by Bead-Spring model with HI, and confirmed that hydrodynamics interaction is very important to accurately model the dynamics of

polymer [9]. In Katz's model, beads are connected with each other by a simple Hooke spring, and the Rotne-Prager tensor along with Lennard-Jones potential is used to simulate HI. Even when HI has been fixed, due to numerical limitation, the bonds (springs) can pass through each other, and hence the topological integrity of a chain is not maintained. Larson and co-workers presented a cross-check process to avoid spring-spring crossing [10]. A FENE spring model is applied in Larson's model, and intromolecular interaction has been separated into two parts, Lennard-Jones potential and a soft potential that presents the repulsive springs. However, Larson did not included HI into his model.

In this study, Larson's Bead-Spring model will be used to capture the feature of a single polymer chain and to investigate the flow induced conformational changes of the polymer by including hydrodynamic interaction of beads.

Chapter 2. Model and Methods

The simplest realization of a Bead-Spring model is to consider only one spring and two beads, known as the Dumbbell Model [11]. Dumbbell model replace the whole chain by a single spring, captures the important physics: chain flexibility and drag due to solvent. It is widely used, but the simple Dumbbell model is not sufficient to indicate the conformation change of the polymer, especially under imposed flow fields [8] [4]. It is necessary to have multiple beads connected with multiple springs, and to include complete solvent effects.

The following effects are primary important for rheological properties, ordered based on their importance [12].

(1) Viscous drag

(2) Entropic elasticity

(3) Brownian forces

(4) Hydrodynamics interaction (HI)

(5) Excluded-volume (EV) interactions

(6) "Internal viscosity" (IV) and

(7) "Self-entanglement" (SE)

Effects (1) to (4) are the essential parts of the polymer dynamics, and they will be discussed later. EV interactions present the repulsive forces between beads that prevent their overlap, which can be cancelled out in some solvent under their theta temperature, at which the repulsion is weak enough compared with effect of the solvent [13]. Although few investigators have considered IV and SE, it is not

clear about their importance and even reality, and hence these two effects will not be included in this study.

In Bead-Spring chain models, chains consist of N beads connected by N-1 flexible springs. The governing equations in the inertia free limit are obtained by a force balance on each bead:

$$F_i^D + F_i^S + F_i^{In} + F_i^B = 0, \quad i = 1,2,....,N \tag{1}$$

where the subscript i refers the bead number and F^D , F^S , F^{IN} , F^B are the hydrodynamic (viscous) drag force, the spring force, the intermolecular interaction and the Brownian force, respectively.

2.1 Drag force

The hydrodynamic drag force is the friction force that flowing solvent exerts on the polymer and is given by [4],

$$\mathrm{F}_i^D = -\zeta\left(\dot{\mathbf{r}}_i - v_i\right) \tag{2}$$

where ζ is the drag coefficient, $\dot{\mathbf{r}}_i$ is the velocity of the bead and v_i is the undisturbed velocity field at the position of bead i. By assuming that the polymer will not change the flow field, v_i is simplified as the solvent velocity at bead i. $v_i = \kappa \cdot \mathrm{r}_i$, where κ is transpose of the velocity gradient tensor, $\kappa = \left(\nabla \mathrm{u}\right)^T$, and hence,

$$\mathrm{F}_i^D = -\zeta\left(\dot{\mathbf{r}}_i - (\nabla \mathbf{u})^T \cdot \mathbf{r}_i\right) \tag{3}$$

.

After substituting and rearranging, the force balance becomes

$$\dot{\mathbf{r}}_i = (\nabla \mathbf{u})^T \cdot \mathbf{r}_i + \frac{1}{\zeta}\left(F_i^S + F_i^{In} + F_i^B\right) \tag{4}$$

This equation is commonly called a Langevin equation, governing the motion of the particle.

2.2 Spring force

Entropic elasticity is important when the flow is strong enough to stretch or shrink the chain, and spring force is perfect to present such effect. Consider a chain of beads connected by springs, each bead (other than two ends) is bounded by two springs, which leads to the following

$$F_i^S = F_{spring\_i}^S - F_{spring\_i-1}^S, \quad 2 \le i \le N-1 \tag{5}$$

where $F_{spring\_i}^S$ is the force that acts on bead i by spring i. For the end beads,

$$\begin{aligned} F_1^S &= F_{spring\_1}^S \\ F_N^S &= -F_{spring\_N-1}^S \end{aligned} \tag{6}$$

The simplest spring force law is Hookean spring law, a linear spring that is infinitely extensible. The Hookean spring is governed by

$$F_{spring\_i}^S = HQ_i \tag{7}$$

where H is the spring constant, $\mathbf{Q}_i = \mathbf{r}_{i+1} - \mathbf{r}_i$. Two other realistic spring law are commonly used, Warner spring law (finitely extensible nonlinear elastic, FENE)

and Marko-Siggia spring law [14]. Most flexible synthetic polymers and single stranded DNA should be modeled using FENE spring law

$$F^{S}_{spring\_i} = \frac{H\mathbf{Q}_i}{1 - Q^2 / Q_0^2} \tag{8}$$

where Q is the magnitude of $\mathbf{Q}_i$ and Q_0 is the maximum extended length for the spring. Many biopolymers resist local bond torsion (e.g. duplex DNA) and are more appropriate to be described with Marko-Siggia spring law [15]

$$F^{S}_{spring\_i} = \frac{k_B T}{l_p}\left[\frac{1}{4}\left(1 - \frac{Q}{Q_0}\right)^{-2} - \frac{1}{4} + \frac{Q}{Q_0}\right] \tag{9}$$

where l_p is the persistence length.

Since this study considers only a single polymer chain, FENE spring law is more convenient and sufficient. However, it is important to note that parameter in the spring force are directly related to the polymer dynamics [16].

2.3 Brownian force

The Brownian force is taken from a random distribution and fluctuates extremely rapidly. According to fluctuation-dissipation theorem, over a long time scale, the average of the random force should tend to zero; a relationship must exist between Brownian motion and drag, since the rate of Brownian motion reflects the diffusion coefficient, which is related to the drag coefficient [12].

A general form of fluctuation-dissipation theorem is given by,

$$\begin{aligned} \left\langle F_i^B(t) \right\rangle &= 0, \\ \left\langle F_i^B(t) F_i^B(t') \right\rangle &= 6k_B T\zeta\delta(t-t') \end{aligned} \tag{10}$$

where $\delta(t-t')$ is the Dirac delta function. Thus, the Brownian force averaged over a time scale Δt becomes

$$F^B = \left(\frac{6k_B T\zeta}{\Delta t} \right)^{1/2} n \tag{11}$$

where n is a random three-dimensional vector, each component of which is uniformly distributed in the interval [-1, 1] [17].

2.4 Hydrodynamic interaction

Hydrodynamic interaction is the interaction between beads by the solvent. As a bead moves, it exerts a force on the solvent, which changes the velocity field from its undisturbed value v_i, and hence changes the hydrodynamic drag force exerted on other beads. According to Newton's second law, the hydrodynamic drag force is equal and opposite to the hydrodynamic force, and is balanced by all other forces exerted on that bead,

$$-F_i^D = F_i^S + F_i^{In} + F_i^B \tag{12}$$

2.4.1 Diffusion tensor

The velocity disturbance v_i' is a linear function of the hydrodynamic drag force,

$$v_i' = -\mathbf{\Omega}_{ij} \cdot F_j^D = \mathbf{\Omega}_{ij} \cdot \left(F_j^S + F_j^{In} + F_j^B \right) \tag{13}$$

where $\boldsymbol{\Omega}_{ij}$ is the hydrodynamic interaction tensor between two beads. Ermak and McCammon shown that the disturbance velocity can be included into the Langevin equation by introducing $\mathbf{D}_{ij} = \frac{k_B T}{\zeta}\left(\delta_{ij}\mathbf{I} + \zeta\boldsymbol{\Omega}_{ij}\right)$, the diffusion tensor [18]. The stochastic differential equation including HI becomes

$$\dot{\mathbf{r}}_i = (\nabla \mathbf{u})^T \cdot \mathbf{r}_i + \sum_{j=1}^{N} \frac{\partial \mathbf{D}_{ij}}{\partial \mathbf{r}_j} + \sum_{j=1}^{N} \frac{\mathbf{D}_{ij} \bullet \left(F_i^S + F_i^{In}\right)}{k_B T} + \left(\frac{6}{\Delta t}\right)^{1/2} \sum_{j=1}^{i} \boldsymbol{\sigma}_{ij} \bullet \mathbf{n}_j \quad (14)$$

where $\boldsymbol{\sigma}_{ij}$ is the weighting factor and can be related to $\mathbf{D}_{ij}$ by $\mathbf{D}_{ij} = \sum_{l=1}^{N} \boldsymbol{\sigma}_{il} \bullet \boldsymbol{\sigma}_{lj}$. Thus the derivative of $\mathbf{D}_{ij}$ with respect to $\mathbf{r}_j$ is zero,

$$\dot{\mathbf{r}}_i = (\nabla \mathbf{u})^T \cdot \mathbf{r}_i + \cancelto{0}{\sum_{j=1}^{N} \frac{\partial \mathbf{D}_{ij}}{\partial \mathbf{r}_j}} + \sum_{j=1}^{N} \frac{\partial \mathbf{D}_{ij} \bullet \left(F_i^S + F_i^{In}\right)}{k_B T} + \left(\frac{6}{\Delta t}\right)^{1/2} \sum_{j=1}^{i} \boldsymbol{\sigma}_{ij} \bullet \mathbf{n}_j \quad (15)$$

In general, the diffusion tensor $\mathbf{D}$ is complicated because it is related to the instantaneous positions of all beads in a nonlinear way. In polymer modeling, the diffusion matrix is often approximated by its far-field asymptotes [19]. The lowest order of approximation is the Oseen-Burgers tensor [20] [21] [4],

$$\begin{aligned} \mathbf{D}_{ij} &= \frac{k_B T}{6\pi\eta a}\mathbf{I} \\ \mathbf{D}_{ij} &= \frac{k_B T}{8\pi\eta r_{ij}}\left(\mathbf{I} + \frac{\mathbf{r}_{ij}\mathbf{r}_{ij}}{r_{ij}}\right) \end{aligned} \quad (16)$$

where $\mathbf{r}_{ij} = \mathbf{r}_i - \mathbf{r}_j$, and $r_{ij} = \left|\mathbf{r}_{ij}\right|$. When the distance between beads is less than the bead diameter (close to each other), the tensor becomes negative, and the Oseen-

Burgers tensor is then not suitable for Brownian dynamics simulations. The next level of approximation corresponds to the Rotne-Prager tensor [22],

$$\mathbf{D}_{ii} = \frac{k_B T}{6\pi\eta a}\mathbf{I} \tag{17}$$

$$\mathbf{D}_{ij} = \frac{k_B T}{8\pi\eta}\frac{1}{r_{ij}}\begin{cases}\left[\left(1+\frac{2a^2}{3r_{ij}^2}\right)\mathbf{I}+\left(1-\frac{2a^2}{r_{ij}^2}\right)\frac{\mathbf{r}_{ij}\mathbf{r}_{ij}}{r_{ij}^2}\right], & r_{ij} \geq 2a \\ \frac{r_{ij}}{2a}\left[\left(\frac{8}{3}-\frac{3r_{ij}}{4a^2}\right)\mathbf{I}+\frac{r_{ij}}{4a}\frac{\mathbf{r}_{ij}\mathbf{r}_{ij}}{r_{ij}^2}\right], & r_{ij} < 2a \end{cases} \tag{18}$$

As the ratio of bead radius to the distance between beads becomes small, the Rotne-Prager tensor can be reduced to the Oseen-Burgers tensor. Note that free draining (without HI) model can be obtained easily by setting $\mathbf{D}_{ij} = \mathbf{D}_{ii}$.

2.4.2 Intermolecular interaction

As mentioned above, the intermolecular force is the effect exerted on a bead due to the intermolecular interactions from all other beads, including bead-bead interaction and spring-spring repulsion (Larson 2010),

$$\mathbf{F}_i^{In} = \sum_{j\neq i}\left(\mathbf{F}_{i,j}^{BB} + \mathbf{F}_{i,j}^{SS}\right) \tag{19}$$

where $\mathbf{F}_{i,j}^{BB}$ and $\mathbf{F}_{i,j}^{SS}$ are contributions due to bead-bead and spring-spring interactions.

I. Bead-bead interaction

Bead-bead interaction presents the potential between beads, and a Lennard-Jones potential is used to model this interaction,

$$\mathbf{F}_{i,j}^{BB} = \frac{4}{d^{ev}}\left[12\left(\frac{d^{ev}}{r_{i,j}}\right)^{13} - 6\varepsilon\left(\frac{d^{ev}}{r_{i,j}}\right)^{7}\right]\hat{\mathrm{r}}_{ij} \tag{20}$$

where $\hat{\mathrm{r}}_{ij}$ is the unit vector along r_{ij} , ε and d^{ev} are the energy and length parameters.

II. Spring-spring repulsion

In Bead-Spring model, the connections between particles are simplified to springs. In real polymer chain, this connection cannot be broken; however, springs can pass through each other due to finite time step size. In order to eliminate the unrealistic crossing, a spring-spring repulsion is used, which based on the distance of closest approach between springs [10]. Consider two springs referred to as i and j, which have two line equations describing their positions.

$$\begin{aligned}\mathbf{S}_i &= \mathrm{r}_i + p_i\mathbf{Q}_i \\ \mathbf{S}_j &= \mathrm{r}_j + p_j\mathbf{Q}_j\end{aligned} \tag{21}$$

Where p_i and p_j are parameters that indicate scaled position along each spring, from 0 to 1. The distance vector between these lines, $\mathbf{D}_{i,j}$, is given by, $\mathbf{D}_{i,j} = \mathbf{S}_i - \mathbf{S}_j$. By solving the equations $\frac{\partial \mathbf{D}_{i,j}}{\partial p_i} = 0$ and $\frac{\partial \mathbf{D}_{i,j}}{\partial p_j} = 0$, the expressions of p_i and p_j can be obtained which correspond to the distance of closest approach [23].

$$p_i = \frac{1}{2}\frac{\left(\mathbf{r}_i - \mathbf{r}_j\right)\cdot\left(Q_{ij}\mathbf{Q}_j - Q_j^2\mathbf{Q}_i\right)}{Q_i^2 Q_j^2 - Q_{ij}^2}$$
$$p_j = \frac{1}{2}\frac{\left(\mathbf{r}_i - \mathbf{r}_j\right)\cdot\left(Q_i^2\mathbf{Q}_j - Q_{ij}\mathbf{Q}_i\right)}{Q_i^2 Q_j^2 - Q_{ij}^2} \tag{22}$$

where $Q_i^2 = \mathbf{Q}_i \cdot \mathbf{Q}_i$, $Q_j^2 = \mathbf{Q}_j \cdot \mathbf{Q}_j$ and $Q_{ij} = \mathbf{Q}_i \cdot \mathbf{Q}_j$. A soft potential is applied for the repulsive force between springs. A simple lever rules is used to convert the spring force to bead forces. For spring i and spring j, the beads of the first spring are bead i and $i+1$, which experience effects from spring j,

$$\mathbf{F}_{i,j}^{SS} = K \cdot \exp\left(-\kappa D_{i,j}\right)\frac{1-p_i}{D_{i,j}}\mathbf{D}_{i,j}$$
$$\mathbf{F}_{i+1,j}^{SS} = K \cdot \exp\left(-\kappa D_{i,j}\right)\frac{p_i}{D_{i,j}}\mathbf{D}_{i,j} \tag{23}$$

Where K and κ are parameters of the strength and range of the repulsive potential.

Chapter 3. Numerical Approach

In order to solve the Langevin equation, an explicit time-stepping algorithm is used. All of the forces depend on the positions of beads at the beginning of each time interval, and remaining the same during that time-step. Since only finite size of time intervals can be achieved, the choice of Δt is always very important. Different values of Δt (between 10^{-4} - 10^{-6}) have been used in the simulation. Generally, the results are insensitive to the size of the time step. However, in few cases (e.g. large bead number and high shear rate), smaller Δt is required (between 10^{-5} - 10^{-6}) to obtained accurate solutions.

3.1 Dimensionless scale

In this study, variables are made dimensionless by scaling length in units of

$$\sqrt{k_B T / H},$$

force in units of

$$\sqrt{H k_B T}$$

and time in units of

$$\zeta / H .$$

The drag coefficient ζ is defined as

$$\zeta = 6\pi\eta a ,$$

where η denoted the viscosity of the fluid. Weissenberg number is introduced to present the intensity of shear flow [9] [10],

$$Wi = \dot{\gamma}\tau \tag{24}$$

where $\dot{\gamma}$ is the shear rate (in unit of s^{-1}) and τ is the longest relaxation time of the polymer (in unit of s).

3.2 Spring force

By applying of time and length dimensionless units, the dimensionless spring force has the form

$$\mathbf{F}_i^S = \frac{\mathbf{Q}_i}{1 - Q_i^2 / b} \tag{25}$$

with

$$b = HQ_0^2 / k_B T = 3N_{K,s}$$

where $N_{K,s}$ is the number of Kuhn steps in a spring [4]. In this study, b is set to 56, and the fully extended length of each spring becomes 7.5. One main limitation is that the spring force becomes non-positive when the length extends beyond the maximum limit, as displayed in Figure 2.

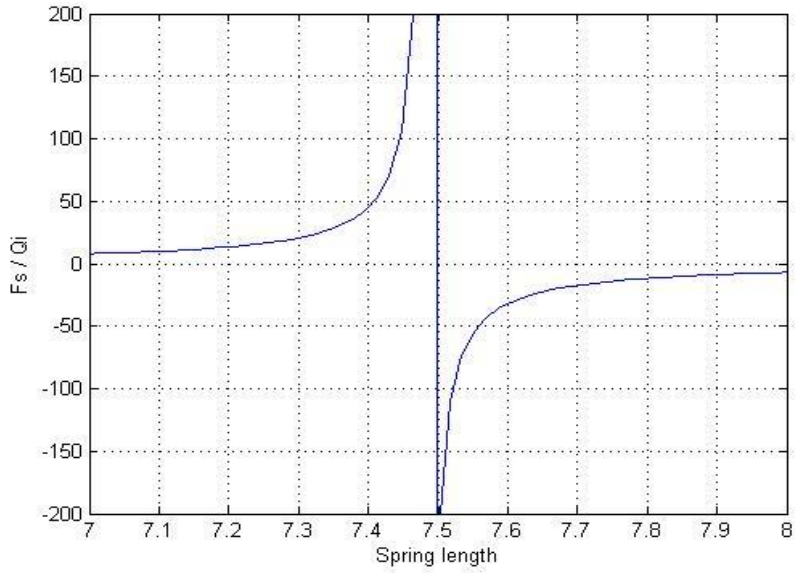

Figure 2 Dependence of the FENE spring force on spring extension

Beyond this limit, the spring becomes repulsive instead of attractive. That will cause further separation of beads. A truncated FENE spring law is used to avoid the switch,

$$\mathbf{F}_i^S = \begin{cases} \dfrac{\mathbf{Q}_i}{1-Q_i^2/b}, & Q_i \le 6.9 \\ \dfrac{\mathbf{Q}_i}{1-0.99^2}, & Q_i > 6.9 \end{cases} \tag{26}$$

.

The depending of spring force on the spring length is illustrated in Figure 3 for a truncated FENE spring law.

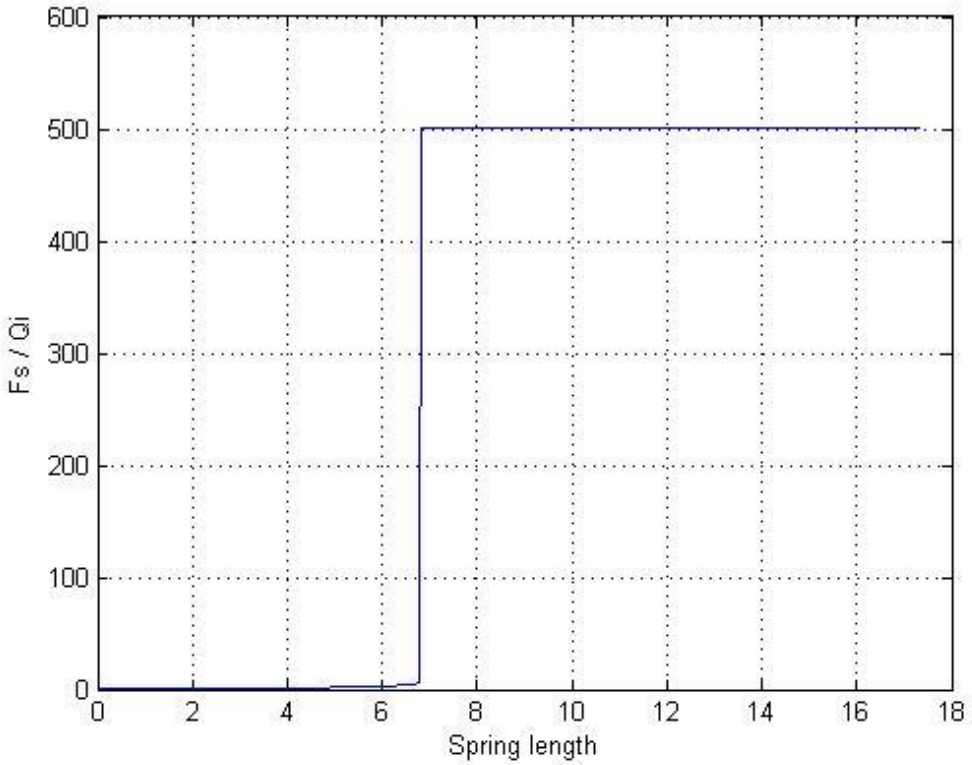

Figure 3 Dependence of the FENE spring force on spring extension with truncated FENE spring law

3.3 Lennard-Jones potential

A truncated Lennard-Jones potential is used to model bead-bead interaction [10]:

$$\mathbf{F}_{i,j}^{BB} = \frac{4}{d^{ev}} \begin{cases} \left[12\left(\frac{d^{ev}}{r_{i,j}} \right)^{13} - 6\varepsilon \left(\frac{d^{ev}}{r_{i,j}} \right)^{7} \right] \hat{\mathrm{r}}_{ij}, & r_{ij} \geq 0.675 \\ \left[12\left(\frac{d^{ev}}{0.675} \right)^{13} - 6\varepsilon \left(\frac{d^{ev}}{0.675} \right)^{7} \right] \hat{\mathrm{r}}_{ij}, & r_{ij} < 0.675 \end{cases} \tag{27}$$

Where $\hat{\mathrm{r}}_{ij}$ is the unit vector along r_{ij}, and ε and d^{ev} are the energy and length parameters. The reason using a truncated potential is that when beads are very close to each other, the standard Lennard-Jones model leads to an unrealistically high potential, as shown in Figure 4.

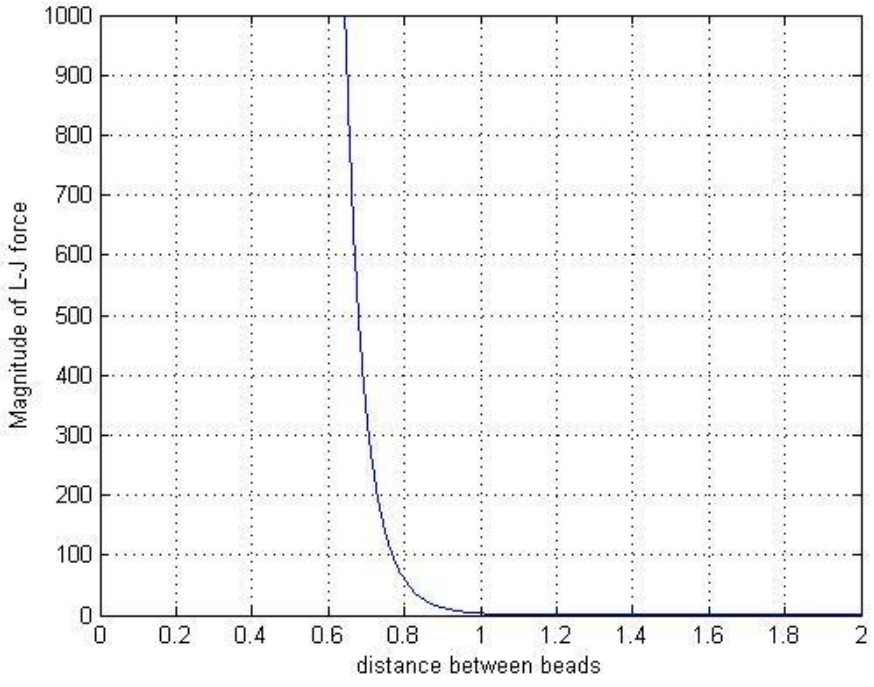

Figure 4 Dependence of the LJ potential force on the distance between beads

Due to the computational limitation, finite time step size makes it impossible to capture and update the potential energy timely. In this case, the simulation would be defective by unrealistic level of potentials at the beginning of a time step. The modified Lennard-Jones force has a "cut-off" point after which the force will become independent of the separation distance between beads, as depicted in Figure 5.

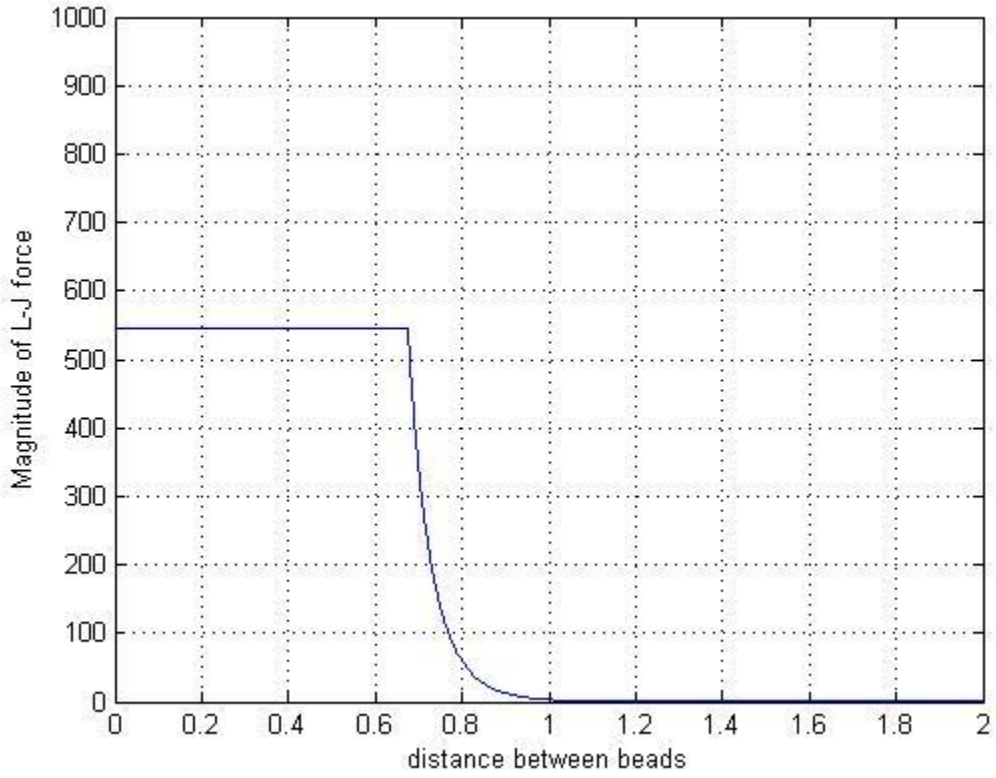

Figure 5 Dependence of the truncated LJ potential force on the distance between beads

3.4 Random force generator

Brownian force is taken from a random distribution, however, "random" is practically impossible to achieve. In numerical computation, random function depends on environment variables, such as CPU clock or other processor-dependent values, and it always has a period. In this study, *call Random_Number ()* is used to generate the random vector, distributed in [0, 1]. This function of Intel FORTRAN Compiler has two separate congruential generators together to produce a period of approximately 10^{18}. By mapping the range to [-1, 1], the random vector has the distribution:

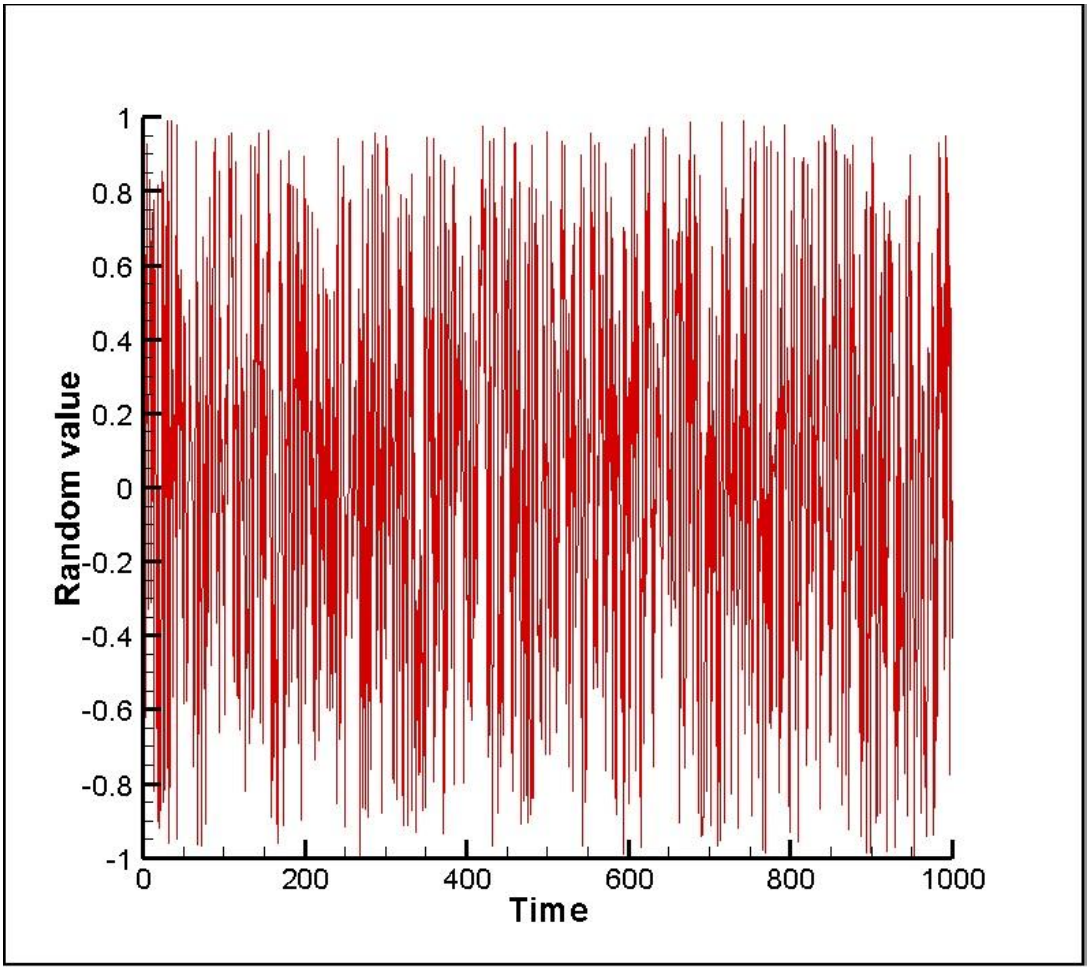

Figure 6 Distribution of one thousand random value generated by *call Random_Number()*

3.5 Cross elimination process

3.5.1 Cross check

To completely avoid spring-spring crossing, a time-stepping algorithm is used [23]. First, a trial move is made with the original time step; a check is then made as to whether any pairs of springs crossed during this time step. The checking process is done by solving the equation

$$\mathbf{S}_i\left(t+\alpha_{ij}\Delta t\right)=\mathbf{S}_j\left(t+\alpha_{ij}\Delta t\right) \tag{28}$$

which assumes that two springs cross at time $t+\alpha_{ij}\Delta t$. Utilizing x and y components, expressions for p_i and p_j are developed

$$p_i=\frac{\left(x_j-x_i\right)\left(y_{j+1}-y_j\right)-\left(y_j-y_i\right)\left(x_{j+1}-x_j\right)}{\left(x_{i+1}-x_i\right)\left(y_{j+1}-y_j\right)-\left(y_{i+1}-y_i\right)\left(x_{j+1}-x_j\right)} \tag{29}$$

$$p_j=\frac{\left(x_j-x_i\right)\left(y_{i+1}-y_i\right)-\left(y_j-y_i\right)\left(x_{i+1}-x_i\right)}{\left(x_{i+1}-x_i\right)\left(y_{j+1}-y_j\right)-\left(y_{i+1}-y_i\right)\left(x_{j+1}-x_j\right)} \tag{30}$$

It is also assumed that the beads move linearly during the time step $\left[t,t+\Delta t\right]$; thus, the positions of each bead can be obtained from

$$\mathbf{r}_i\left(t+\alpha_{ij}\Delta t\right)=\mathbf{r}_i\left(t\right)+\alpha_{ij}\left(\mathbf{r}_i\left(t+\Delta t\right)-\mathbf{r}_i\left(t\right)\right) \tag{31}$$

with $0\le\alpha_{ij}\le1$. Substitution p_i, p_j and the linear motion equation into the line equation give the following cubic equation in α_{ij},

$$
\begin{aligned}
&\left(x_{j,i}+\alpha_{ij}\Delta x_{j,i}\right)\left(y_{j+1,j}+\alpha_{ij}\Delta y_{j+1,j}\right)\left(z_{i+1,i}+\alpha_{ij}\Delta z_{i+1,i}\right)\\
&+\left(x_{i+1,i}+\alpha_{ij}\Delta x_{i+1,i}\right)\left(y_{j,i}+\alpha_{ij}\Delta y_{j,i}\right)\left(z_{j+1,j}+\alpha_{ij}\Delta z_{j+1,j}\right)\\
&+\left(x_{j+1,j}+\alpha_{ij}\Delta x_{j+1,j}\right)\left(y_{i+1,i}+\alpha_{ij}\Delta y_{i+1,i}\right)\left(z_{j+1,j}+\alpha_{ij}\Delta z_{j+1,j}\right)\\
&-\left(x_{j,i}+\alpha_{ij}\Delta x_{j,i}\right)\left(y_{i+1,i}+\alpha_{ij}\Delta y_{i+1,i}\right)\left(z_{j+1,j}+\alpha_{ij}\Delta z_{j+1,j}\right)\\
&-\left(x_{j+1,j}+\alpha_{ij}\Delta x_{j+1,j}\right)\left(y_{j,i}+\alpha_{ij}\Delta y_{j,i}\right)\left(z_{i+1,i}+\alpha_{ij}\Delta z_{i+1,i}\right)\\
&-\left(x_{i+1,i}+\alpha_{ij}\Delta x_{i+1,i}\right)\left(y_{j+1,j}+\alpha_{ij}\Delta y_{j+1,j}\right)\left(z_{j,i}+\alpha_{ij}\Delta z_{j,i}\right)=0
\end{aligned}
\tag{32}
$$

where

$$x_{j,i}=x_j(t)-x_i(t)$$

$$\Delta x_{j,i}=\left[x_j\left(t+\Delta t\right)-x_j\left(t\right)\right]-\left[x_i\left(t+\Delta t\right)-x_i\left(t\right)\right].$$

y- and z-components are analogous. By solving the above equation, three parameters are obtained, α_{ij}, p_i and p_j. If all of these three parameters lie between 0 and 1, the two springs intersected in the preceding time step. The intersection point will be $\mathrm{r}_i+p_i\mathbf{Q}_i$ for spring i; $\mathrm{r}_j+p_j\mathbf{Q}_j$ for spring j, and the intersection happen at the time of $t+\alpha_{ij}\Delta t$. After establishing the values of α_{ij} for different spring pairs, the time step for the real move is then set to $\alpha_{\min} f\Delta t$, where $\alpha_{\min}=\min(\alpha_{ij})$ and f is a factor which is less than 1. The above adaptive time step ensures no spring pairs cross; each new time step resets the original time step and begins the new process.

3.5.2 Spring-Spring repulsion force

To completely eliminate spring cross, a soft potential is applied as the interaction between each spring, and this force is converted into bead forces by a lever rule [12]. The force between each two springs will become four forces on each end of the springs. The forces on spring i due to repulsion from spring j is given by

$$\begin{aligned} \mathrm{F}_{i,j}^{SS} &= K\exp(-\kappa D_{i,j})\frac{1-p_i}{D_{i,j}}\mathbf{D}_{i,j} \\ \mathrm{F}_{i+1,j}^{SS} &= K\exp(-\kappa D_{i,j})\frac{p_i}{D_{i,j}}\mathbf{D}_{i,j} \end{aligned} \tag{33}$$

Where K and κ determine the strength and range of the repulsive potential. In this study, K is set to 2 and κ is 0.25.

3.6 Explicit time-stepping method

The ideal simulation method is updating all of the information timely, however, due to numerical limitation; data can only be obtained after each time step. An explicit time-stepping method is used in the simulation, by updating all of the variables at the beginning of each time step and assuming unchanged during each time step.

$$\frac{\mathbf{r}_i-\mathbf{r}_i^{old}}{\Delta t}=(\nabla\mathbf{u})^T\cdot\mathbf{r}_i^{old}+\sum_{j=1}^{N}\frac{\mathbf{D}_{ij}\bullet\left(F_i^S+F_i^{In}\right)}{k_BT}+\left(\frac{6}{\Delta t}\right)^{1/2}\sum_{j=1}^{i}\boldsymbol{\sigma}_{ij}\bullet\mathbf{n}_j \tag{34}$$

By applying dimensionless units of length, force and time, and using an explicit time-stepping method, the Langevin equation can be rearranged as

$$\mathbf{r}_i=\mathbf{r}_i^{old}+\left[(\nabla\mathbf{u})^T\cdot\mathbf{r}_i^{old}+\sum_{j=1}^{N}\mathbf{D}_{ij}\bullet\left(\mathbf{F}_i^S-\mathbf{F}_{i-1}^S+\mathbf{F}_{i,j}^{BB}+\mathbf{F}_{i,j}^{SS}\right)\right]\Delta t+\left(6\Delta t\right)^{1/2}\mathbf{n}_i \tag{35}$$

Chapter 4. Result and discussion

In this study, chains are modeled by combining different interactions. Since the spring force and the Brownian dynamic force are the most components in bead-spring model, these two interactions will be included in all of the simulations.

In each simulation, 25 different initial conformations are used to reduce the influence of randomness and improve the statistics. The initial conformations are generated by placing the first bead at the origin and subsequent beads at random locations $\sqrt{3}$ away from the preceding one.

Simulations explore the use of different time step Δt (between $10^{-4} - 10^{-6}$), time step selection is dependent upon flow conditions modeled. Typically, the higher the flow rate, the smaller Δt required; most simulations conducted here utilized time step size $\Delta t = 10^{-4}$. Total time steps used in the simulation is at least 2×10^7, with the first 10^6 time steps worth of data discarded to allow the system to reach steady state. The data obtained for first 10^6 time steps is excluded in calculating the time averaged proper of system.

The radius-of-gyration is used to present the conformation of the polymer chain,

$$R_g = \sqrt{\frac{\left\langle \sum_{i=1}^{N} \left| \mathbf{r}_i - \mathbf{r}_{c.m.} \right|^2 \right\rangle}{N}} \tag{36}$$

where r_i is the position of ith bead, $r_{c.m.}$ is the center of mass of the chain and $\langle . \rangle$ denotes an ensemble average.

4.1 Free draining

In the free draining fluid field, hydrodynamics interaction (HI) is neglected. Chains are modeled with different combinations of interactions in quiescent solvent or in flow. Bead volumes are not considered. However, as an important part in HI model, the relationship between bead radius and radius-of-gyration is significant. Simulations with different bead radius are included when HI is included in the model.

4.1.1 No shear flow

Temporal characteristics R_g are displayed in Figure 7 for the radius-of-gyration as a function of time for a 20-bead chain in no flow condition: (a) no interaction, (b) Lennard-Jones (LJ) potential (bead-bead interaction), (c) spring-spring (SS) repulsion and (d) both spring-spring repulsion and Lennard-Jones potential. Data are stored every 50000 time steps, thus 400 data points lead to 2×10^7 time steps. Averages are taken over the second half of the whole simulations, 10^7 time steps, with the first 10^7 time steps discarded for equilibration.

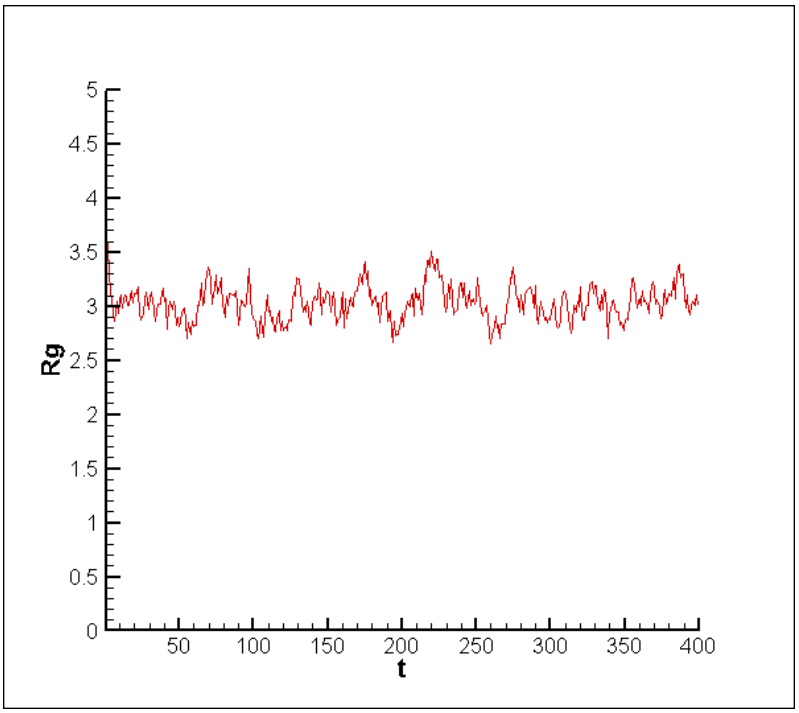

Figure 7(a) Time dependence of no interaction case for a 20-bead chain

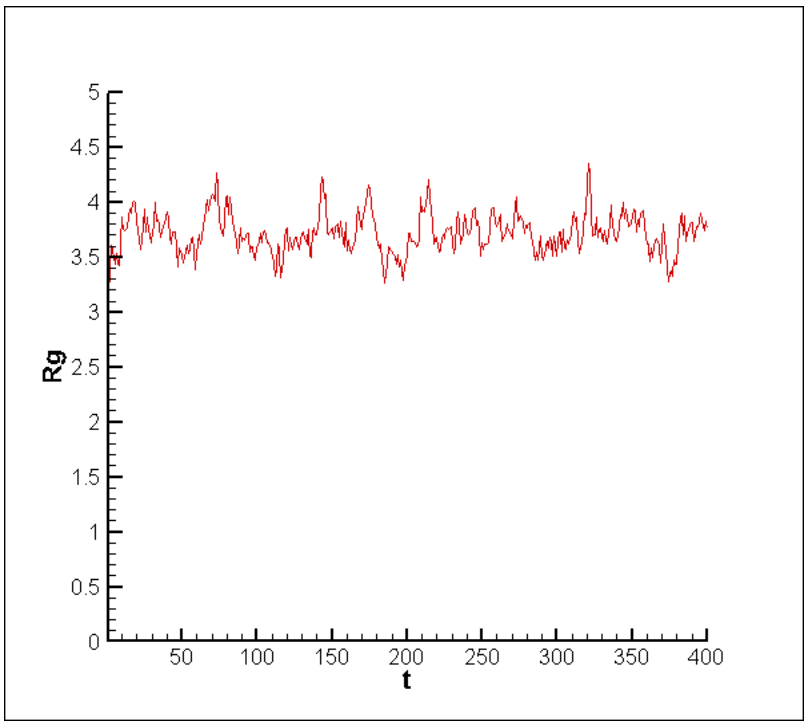

Figure 7(b) Time dependence of LJ case for a 20-bead chain

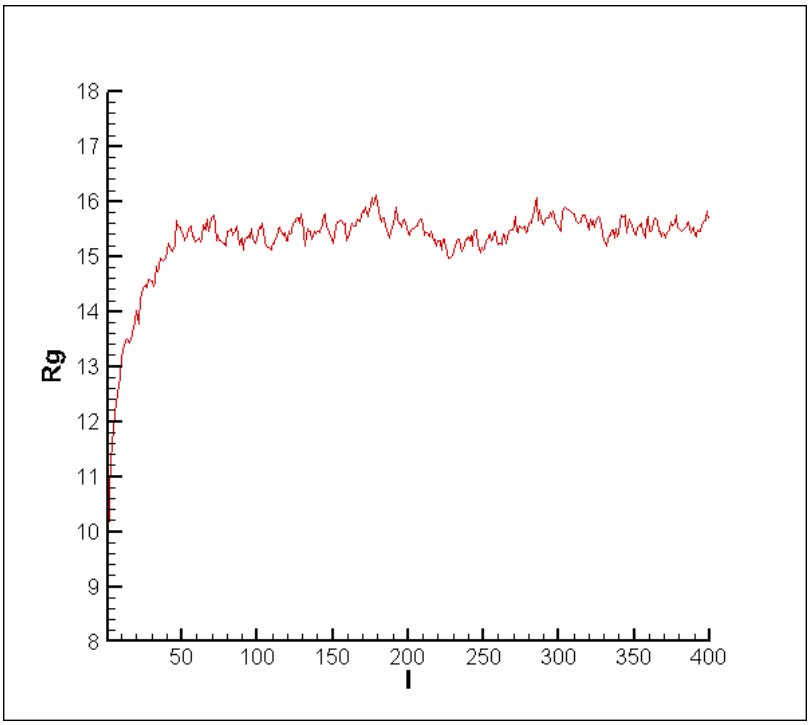

Figure 7(c) Time dependence of SS case for a 20-bead chain

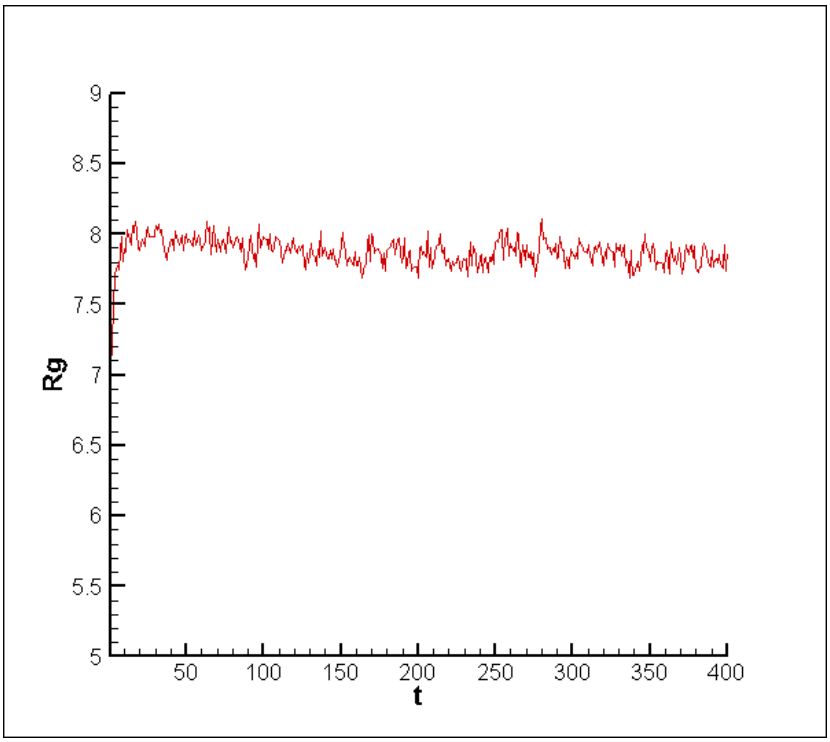

Figure 7(d) Time dependence of SS & LJ case for a 20-bead chain

Figure 8 shows the dependence of the radius-of gyration on length in no flow condition. The cases where spring-spring repulsions are not included are plotted in Fig.8 (a). The results are obtained with and without Lennard-Jones potential. The Lennard-Jones parameters are $d^{ev} = 0.8$ and $\varepsilon = 0$. R_g versus bead number (N) including Spring-spring repulsions with and without LJ bead interaction are displayed in Fig.8 (b). The parameters are $K = 2$ and $\kappa = 0.25$, and $d^{ev} = 0.8$ and $\varepsilon = 5.6$. By comparing Figs.8 (a) and 8 (b), it is apparent that both the absolute coil size for a given chain length and the difference in coil size are larger when spring-spring repulsion are. Due to the size of computation, simulations with SS only consider up to 50 beads.

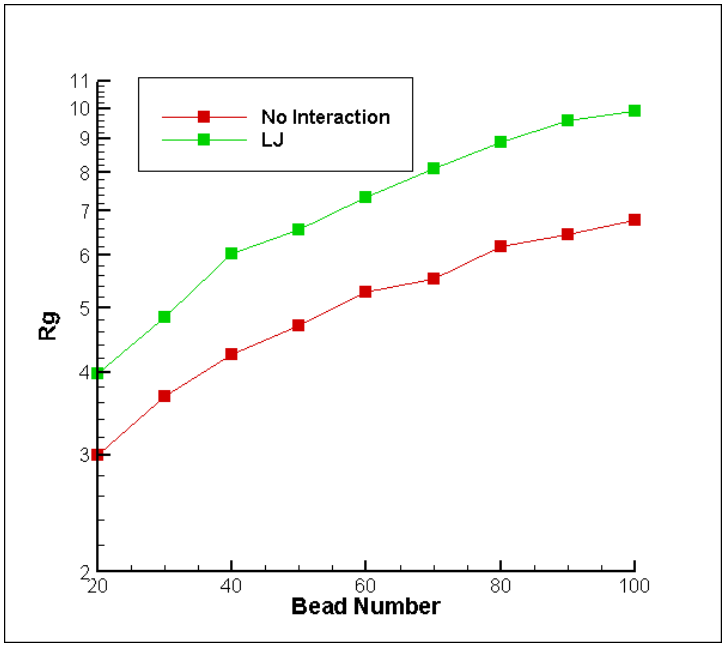

Figure 8(a) Dependence of the radius-of-gyration R_g on chain length N without spring-spring repulsions

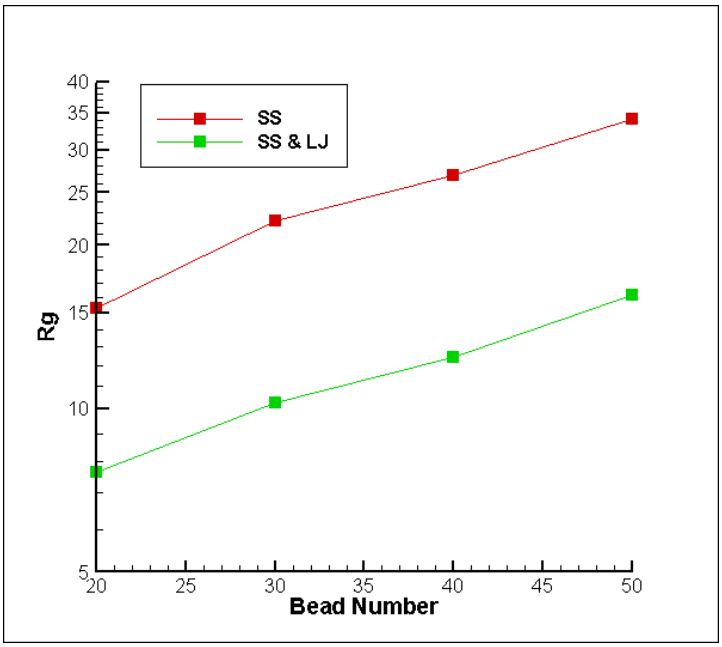

Figure 8(b) Dependence of the radius-of-gyration R_g on chain length N without spring-spring repulsions

Figure 9 shows the conformation of the chain before and after the simulations with different combinations of interactions. As shown in the Fig. 9(c), spring-spring repulsions play a significant part in the simulation. When spring-spring repulsion is included without LJ potential, the chain is unfolding even without flow. One possible reason is that the strength and range parameter are not chosen appropriately, which makes the repulsions slightly too strong, compared with spring force or Brownian dynamics force. Fig. 9(b) and 9(d) show the results with LJ potential. Since $\varepsilon = 0$ in Fig. 9(b) while $\varepsilon = 5.6$ in Fig. 9(d), LJ potential change from repulsion (Fig. 9(b)) to attraction (Fig. 9(d)).

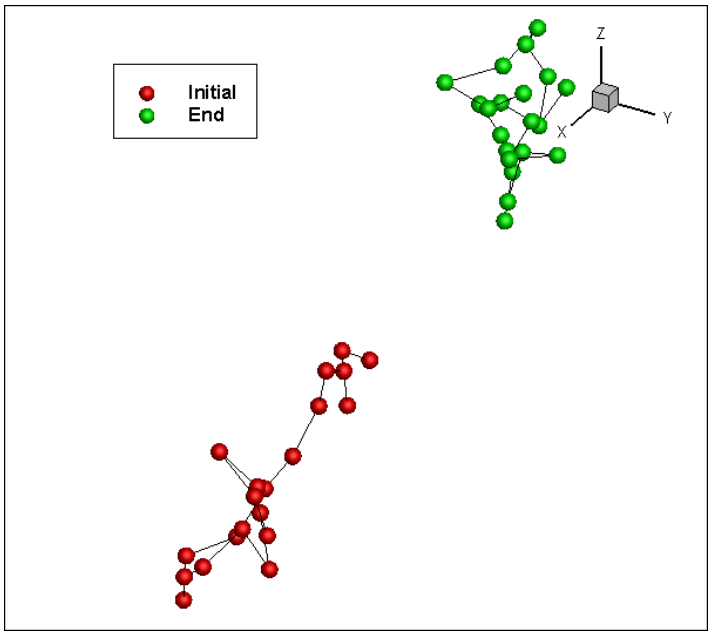

Figure 9(a) Snapshots showing the conformation of the chain at the initial and at the end of the simulation without intermolecular interactions

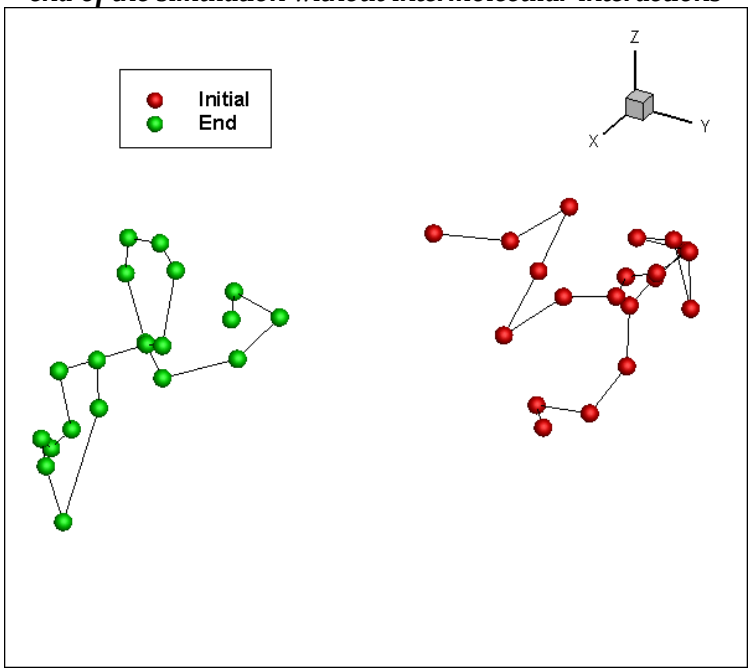

Figure 9(b) Snapshots showing the conformation of the chain at the initial and at the end of the simulation with LJ potential when $d^{ev} = 0.8$ ***and*** $\varepsilon = 0$ **.**

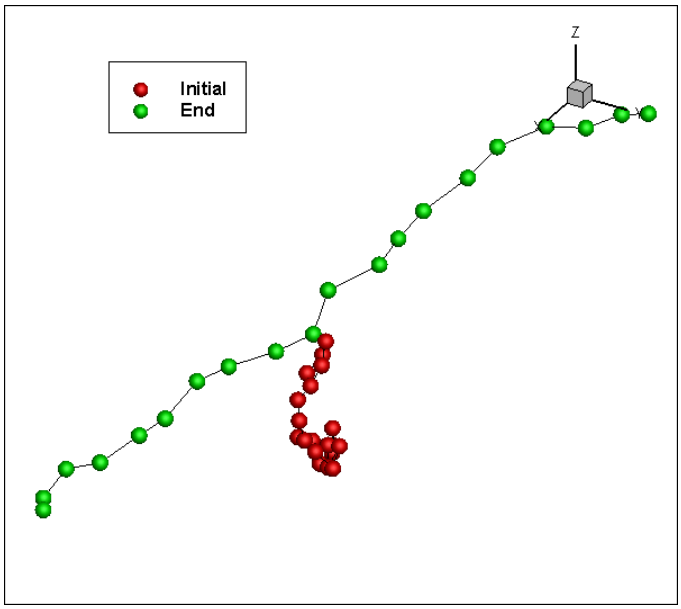

Figure 9(c) Snapshots showing the conformation of the chain at the initial and at the end of the simulation with spring-spring repulsion when $K = 2$ ***and*** $\kappa = 0.25$.

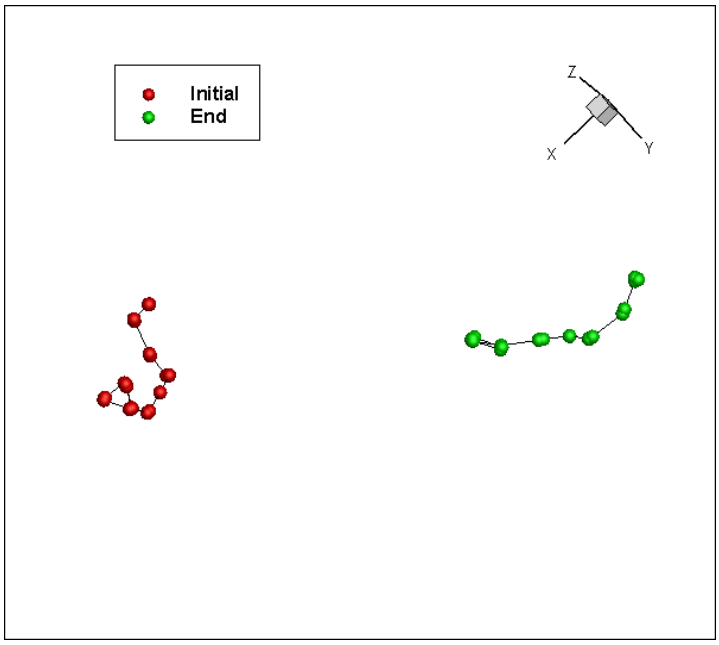

Figure 9(d) Snapshots showing the conformation of the chain at the initial and at the end of the simulation with both LJ potential when $d^{ev} = 0.8$ ***and*** $\varepsilon = 5.6$ ***and spring-spring repulsion when*** $K = 2$ ***and*** $\kappa = 0.25$.

4.1.2 Shear flow

In this part, a polymer chain is placed in a simple shear flow. The velocity gradient of the flow field is given by

$$\nabla \mathbf{u} = \begin{pmatrix} 0 & 0 & \dot{\gamma} \\ 0 & 0 & 0 \\ 0 & 0 & 0 \end{pmatrix},$$

and $\dot{\gamma}$ is the shear rate. Weissenburg number (Wi) is used to present the intensity of shear flow, $Wi = \tau\dot{\gamma}$, where τ is the longest relaxation time of a polymer chain. The relaxation time is obtained by

$$\tau = \frac{\zeta}{8H \sin^2(\pi / 2N)} \tag{37}$$

.

For a 20-bead chain, the longest relaxation time τ is 20.3 in units of ζ / H.

Figure 10 shows the convergence of the radius-of-gyration for a 20-bead chain at Weissenberg number $Wi = 10$: (a) no interaction, (b) LJ potential (bead-bead interaction). Averages are taken over the last quarter of the whole simulations, a total number of 2×10^7 time steps is used in simulations. Transient response of the polymer chain in flow in much longer than that of the polymer chain in quiescent solvent.

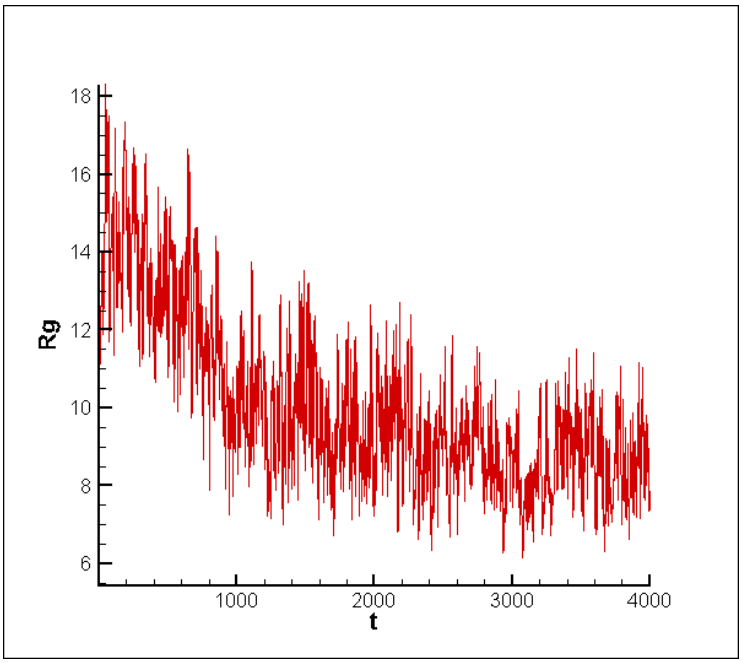

Figure 10 (a) Time dependence of no interaction case for a 20-bead chain at $Wi = 10$

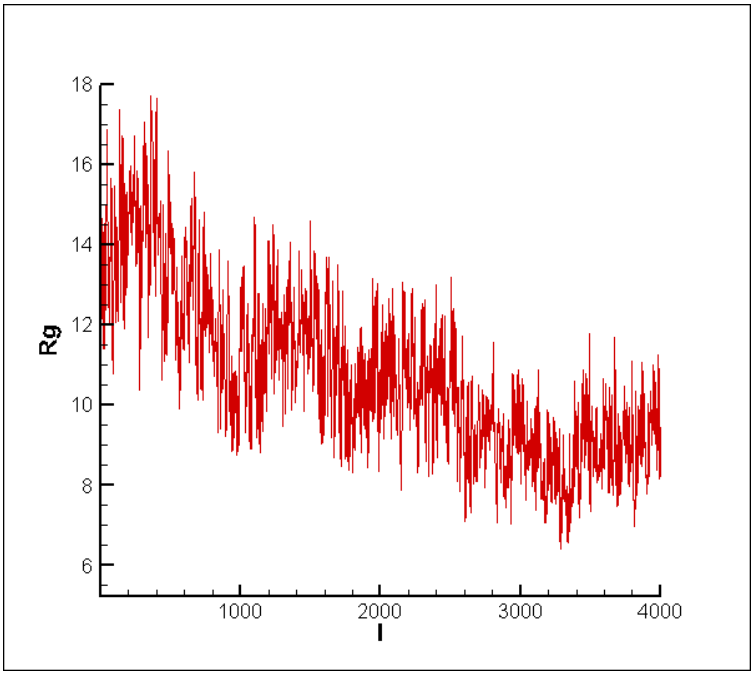

Figure 10 (b) Time dependence of LJ case for a 20-bead chain at $Wi = 10$

Figure 11 displays the ensemble average of R_g as a function of *Wi* with and without the bead-bead interaction. At a fixed *Wi*, R_g is larger when LJ potential is included as repulsion, but with the increasing of *Wi*, the difference between with and without LJ potential is decreasing. The impact of LJ potential is relatively small when there is a shear flow with high shear rate, as shown in Figure 11. In both cases, unfolding happen when *Wi* is around 1, and completely unfolded when *Wi* is greater than 10. The conformations of each case on $Wi = 1$ and $Wi = 10$ are shown in figure 12 and 13. Despite the chains are unfolded on $Wi = 10$ in both cases, the coil size is larger when LJ potential is included. There is a clear transition in conformations of the polymer chain occurring *Wi* around unity for both cases (with and without LJ bead interaction).

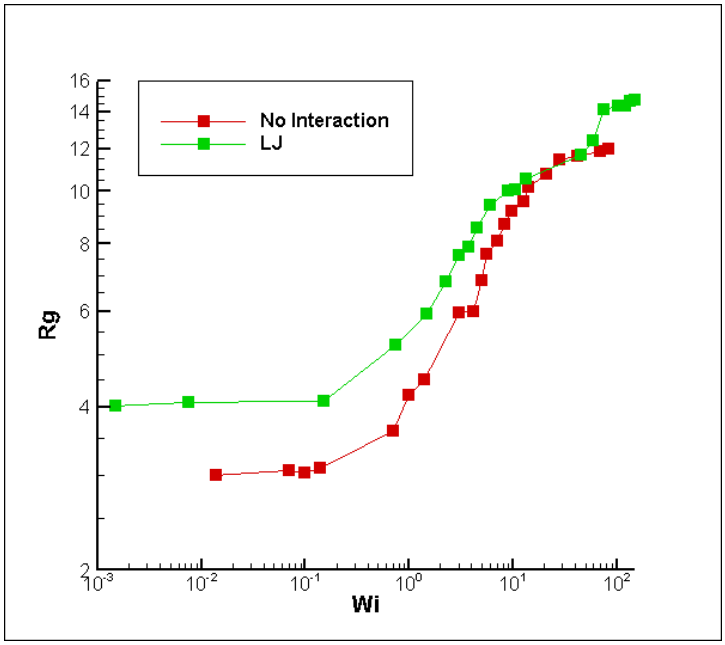

Figure 11 Dependence of the radius-of-gyration R_g for a 20-bead chain at Weissenberg number Wi

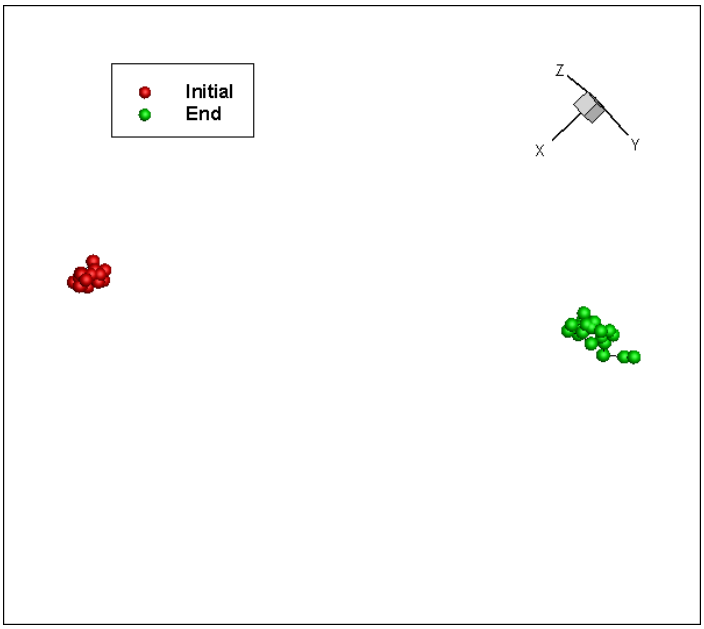

Figure 12(a) Snapshots showing the conformation of the chain at the initial and at the end of the simulation without intermolecular interactions at $Wi = 1$

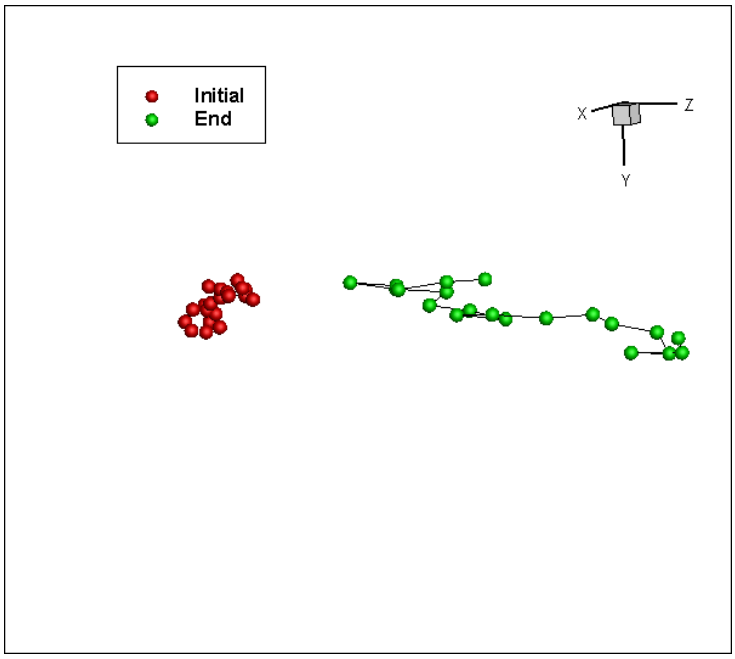

Figure 12(b) Snapshots showing the conformation of the chain at the initial and at the end of the simulation without intermolecular interactions at $Wi = 10$

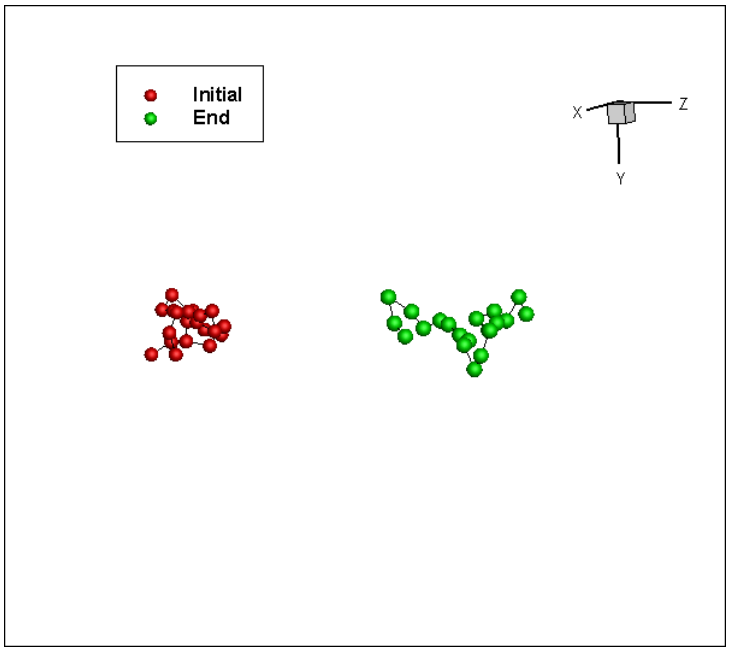

Figure 13 (a)Snapshots showing the conformation of the chain at the initial and at the end of the simulation with LJ potential at $Wi = 1$

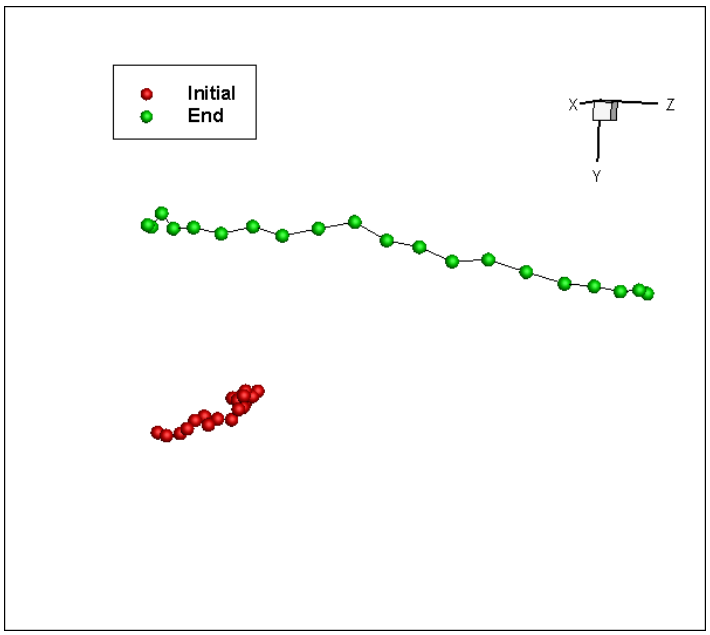

Figure 13 (b) Snapshots showing the conformation of the chain at the initial and at the end of the simulation with LJ potential at $Wi = 10$

4.1.3 Modification of considering radius

Since HI model is based on the Rotne-Prager tensor, which requires a non-zero volume fir beads, it is important to test the effect of bead radius on the conformational behavior of the polymer chain before it is included in HI model. Based on the maximum length of each spring, bead radius should be in the range of 0.1 to 0.5.

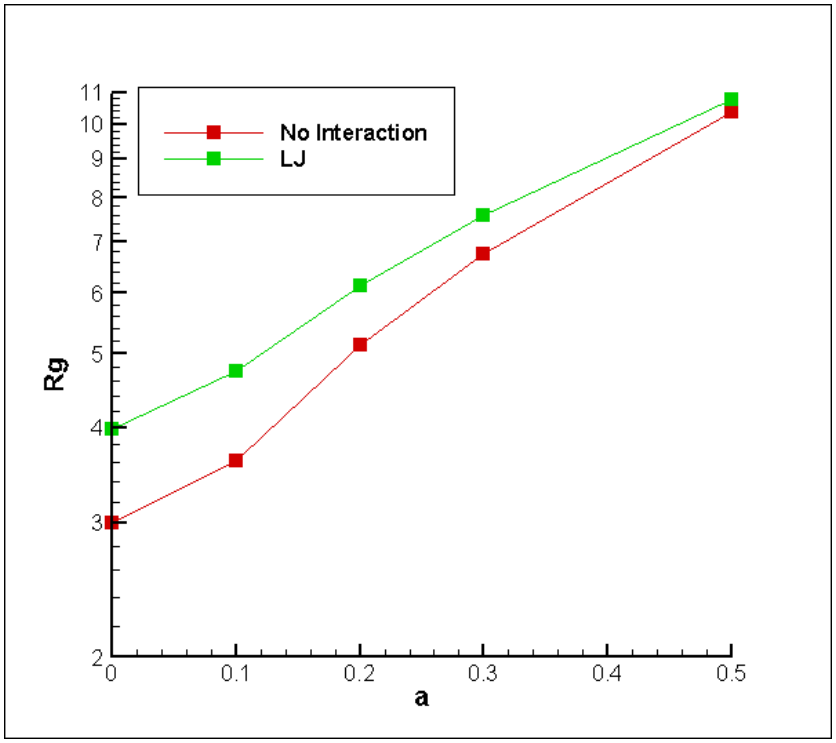

Figure 14 Dependence of the radius-of-gyration R_g for a 20-bead chain on the bead radius

The equilibrium end-to-end distance of each spring is kept constant while the bead radius is varied. It is reasonable that R_g increases with the increasing bead radius while the impact of LJ potential decreases. Since LJ potential is short-range

repulsion, the magnitude of LJ decreases when the distance between the center of mass of each bead increases.

4.2 Hydrodynamics interaction model

Next, hydrodynamics interaction will be included into the simulations. As discussed earlier, bead radius is an important part of HI. Katz and his colleagues simulated HI by using the Rotne-Prager tensor. The present study employs the Rotne-Prager tensor as well to model HI. Due to different length scale and different spring-bead model, their choice of bead radius may not be appropriate for this study. The Lennard-Jones potential used by Katz and his co-workers is $U_{LJ} = \varepsilon k_B T \sum_{ij} \left(\left(2a / r_{ij} \right)^{12} - 2\left(2a / r_{ij} \right)^{6} \right)$, which is very similar to LH bead potential used by the present work. The difference is $2a$ in Katz's model is replaced by d^{ev} in present study. Since d^{ev} is equal to 0.8, a can be simply set as 0.4 to make both LJ bead potential to be identical.

Figure 15 shows the convergence of the radius-of-gyration gyration for a 20-bead chain at Weissenberg number $Wi = 10$: (a) free-draining (FD) cases, (b) hydrodynamics interaction (HI) cases. Transient response of the polymer chain for FD is much shorter than that for HI. Average of R_g is determined over 10^7 time steps for FD while the average of R_g is calculated over 1.25×10^9 time steps when HI is included.

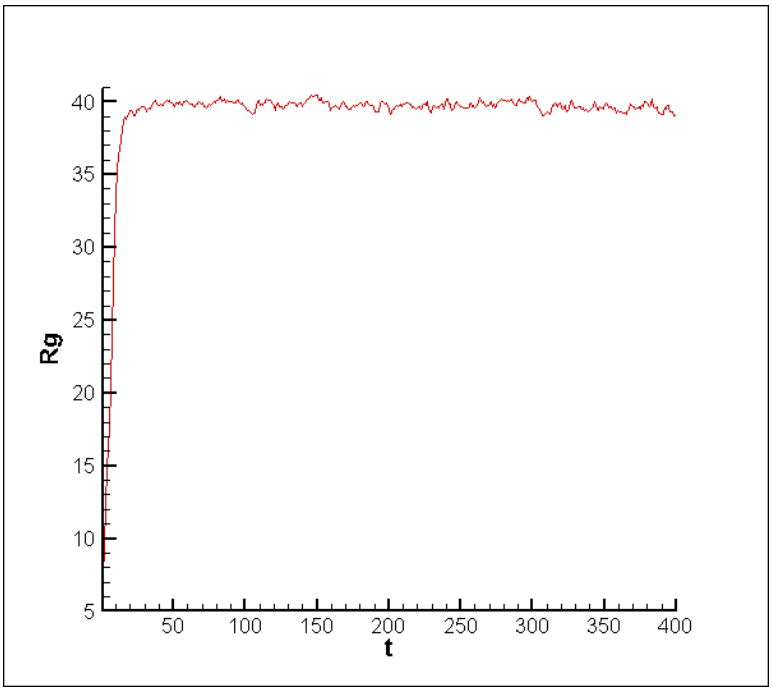

Figure 15(a) Time dependence of FD case for a 20-bead chain at $Wi = 10$

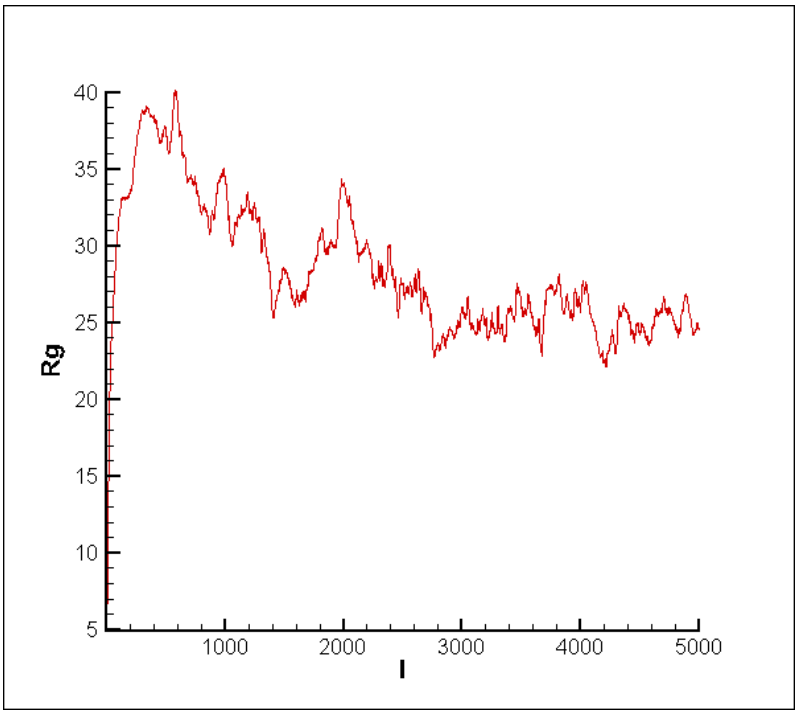

Figure 15(b) Time dependence of HI case for a 20-bead chain at $Wi = 10$

In HI simulations, spring force, Lennard-Jones force and Brownian dynamics force are always included, while spring-spring repulsion is not. The coil size increases in both cases, but HI delays unfolding of the polymer chain. For $Wi < 2$, the coil size of the chain with HI is larger than the one of FD case, and for $Wi > 2$, the coil size of FD case is larger. As seen in Fig. 16, under no or low shear flow, HI serves as repulsive force, intensifying the unfolding process; with the increasing of Wi, HI serves as attractive force at higher shear rates.

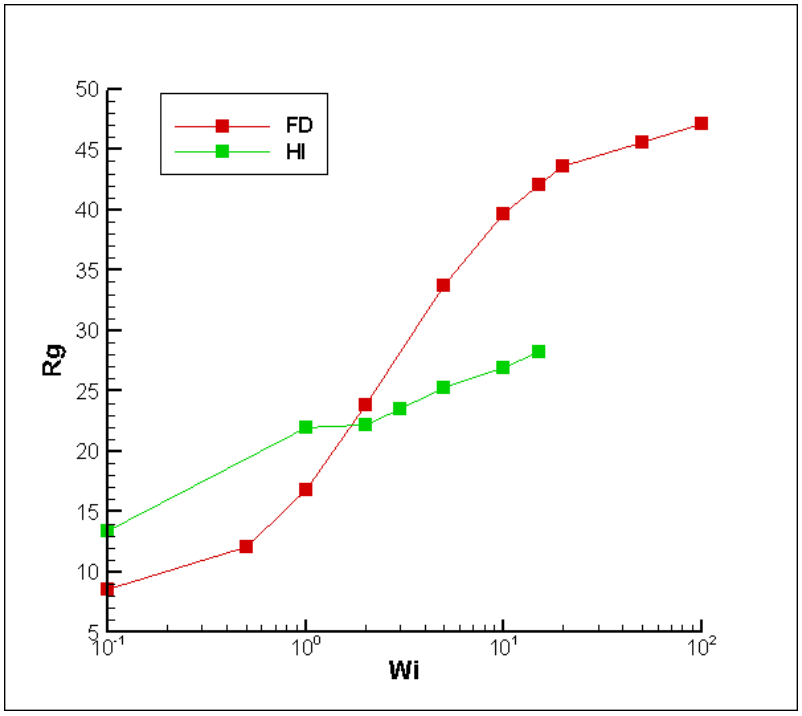

Figure 16 Dependence of the radius-of-gyration R_g for a 20-bead chain at Weissenberg number Wi

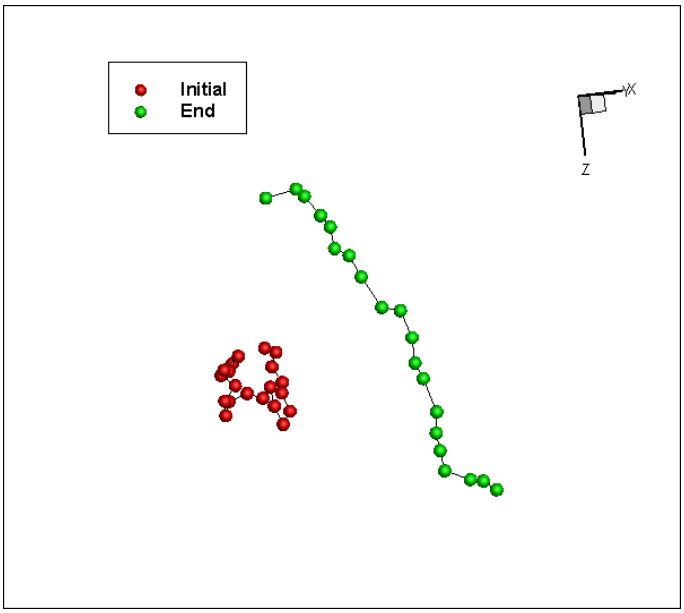

Figure 17(a) Snapshots showing the conformation of the chain at the initial and at the end of the simulation in FD at $Wi = 1$

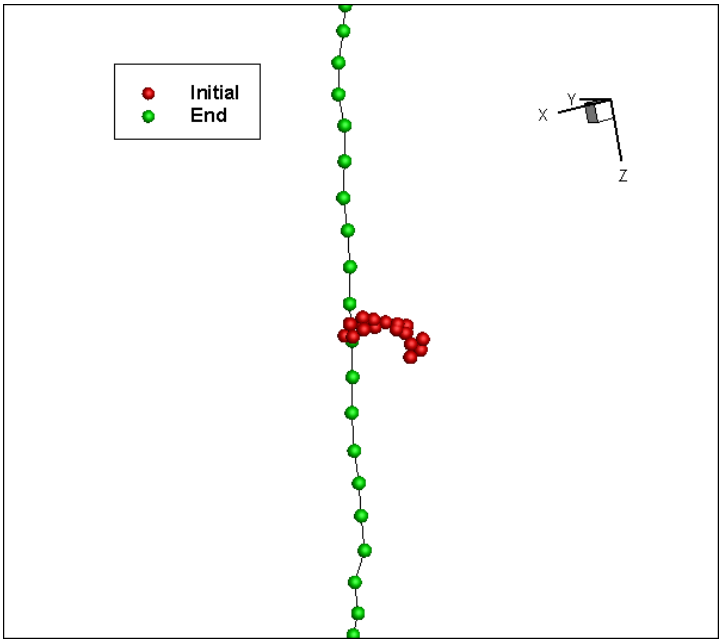

Figure 17(b) Snapshots showing the conformation of the chain at the initial and at the end of the simulation in FD at $Wi = 10$

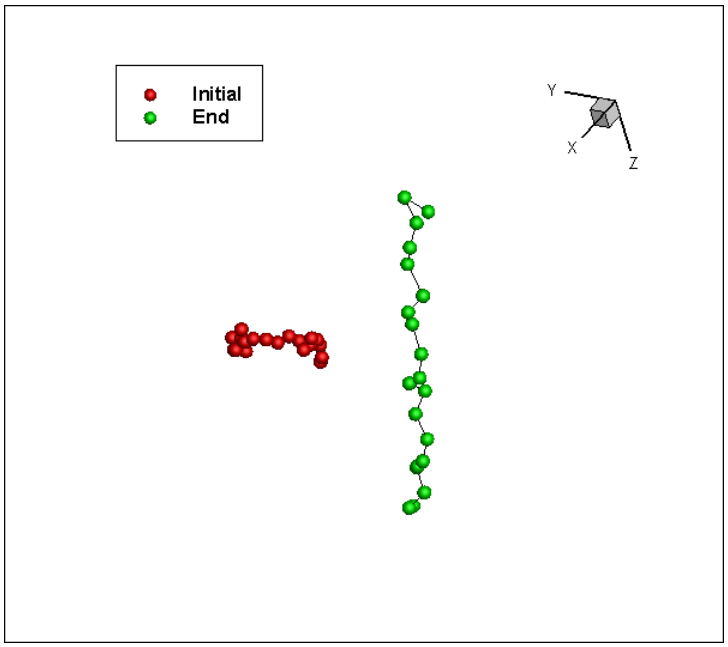

Figure 18(a) Snapshots showing the conformation of the chain at the initial and at the end of the simulation in HI at $Wi = 1$

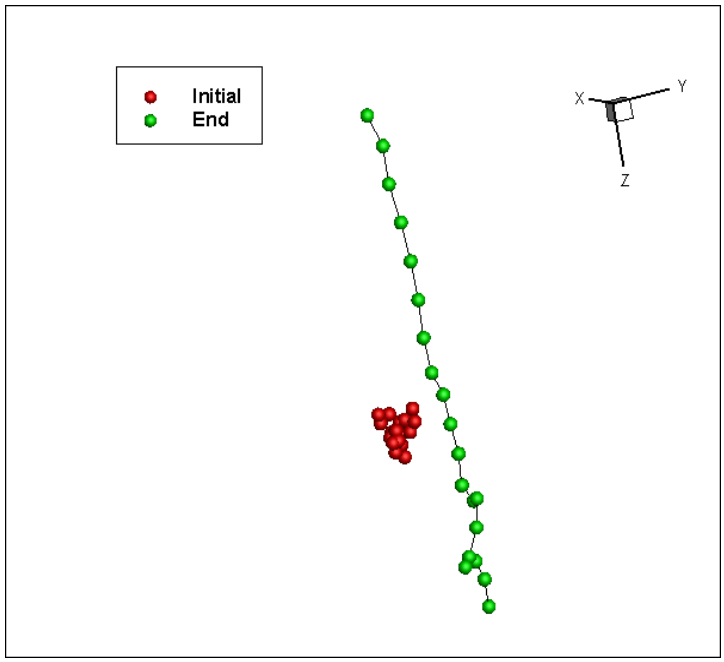

Figure 18(a) Snapshots showing the conformation of the chain at the initial and at the end of the simulation in HI at $Wi = 10$

HI was shown to play a hindering role. A higher shear rate is required to unfold the chains with HI than without. Rzehak first presented this phenomenon in terms of the no-draining effect: the residues hidden inside the protein are shielded from the flow and thus only a small fraction of the residues experience the full drag force. In contrast, this drag force will effect on all residues.

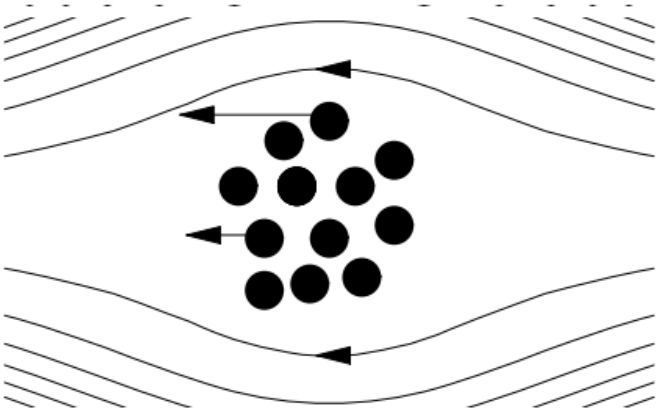

Fig. 4.10 The shielding effect: the particles inside a cluster experience a smaller drag force than those on surface [24]**.**

Chapter 5. Conclusion

5.1 Conclusion

Brownian dynamics simulations of single polymer chains are performed in this study. Four kinds of interactions are discussed, viscous drag, entropic elasticity, Brownian forces and hydrodynamics interaction. The viscous drag force is simulated by Stokes Drag Law, and FENE spring model is applied to as the entropic elasticity. Hydrodynamics interaction is separated into two parts, intermolecular interaction and diffusion tensor. A spring-cross elimination process is included in this study, and spring-spring repulsion is used to avoid the situation that the springs cross each other. Different cases are simulated by using different combination of interactions; spring force and Brownian dynamic force are throughout included.

In free-draining cases, Lennard-Jones potential and spring-spring repulsion are included when needed. Both no flow and shear flow cases are simulated. When the polymer chain is in quiescent solvent, the coil size increases with increasing bead number, and spring-spring repulsion helps the chain to be unfolded. When the polymer chain is in shear flow, LJ bead interaction cause more unfolding of the polymers. The onset of unfolding of the chain is about *Wi* of 1 with or without the LJ bead interaction presents. As the size of bead increases the coil size becomes larger.

To made hydrodynamic interaction, Lennard-Jones force and HI diffusion tensor are considered. Including HI effect is important to model flow induced

conformational changes of biological systems. Due to the shielding effect, the residues hidden inside the protein are shielded from the flow and only a small fraction of residues experience the full drag. When no HI are present, this fraction is applied on all residues [19]. HI were shown to restrain the unfolding, thus a higher intensity of shear flow is required to unfold the chains.

5.2 Future work

Due to the tremendous computing required by spring-cross elimination, this process only presents in FD- no-flow case, and the largest bead number simulated is 50. It will be interesting to see how the inclusion of spring-cross elimination process affects the HI simulations.

It is still not clear how other flow field will affect the chains. Mr. Wenli Ouyang and Mr. Haolin Ma from Lehigh University are simulating polymer behavior near wall or inside a cavity. Boundary effect can be included into the simulations along with HI and/or spring-cross elimination.

This study is focused on the simulations of single polymer chain, and it will be interesting to have multi-chain simulations. These simulations require even more computer resources, and it cannot be done until parallel computing embedded.

Finally, conformational changes of a single chain polymer in shear flow is studied here. It is also important to understand how the dynamics of the polymer chain in extensional flows and in combination of shear and extensional flows.

Bibliography

[1] A. Kaushansky, "Quantifying protein–protein interactions in high throughput using protein domain microarrays," *Nature Protocols,* pp. 773 - 790, 2010.

[2] J. E. Sadler, "New Concepts in Von Willebrand Disease," *Annual Review of Medicine,* vol. 56, pp. 173-191, 2005.

[3] E. P. Widmaier, Outlines & Highlights for Vander's Human Physiology, AIPI, 2011.

[4] R. B. Bird, Dynamics of polymeric liquids, Vol.2, Wiley, 1977.

[5] T. Perkins, "Stretching of a Single Tethered Polymer in a Uniform flow," *Science,* vol. 268, pp. 83-87, 1995.

[6] A. Peterlin, "Hydrodynamics of macromolecules in a velocity field with longitudinal gradient," *Journal of Polymer Science* , vol. 4, no. 4, pp. 287-291, 1966.

[7] O. Kratky, G. Porod, "Röntgenuntersuchung gelöster Fadenmoleküle," *Recueil des Travaux Chimiques des Pays-Bas,* vol. 68, no. 12, pp. 1106-1122, 1949.

[8] P. E. Rouse, "A Theory of the Linear Viscoelastic Properties of Dilute Solutions of Coiling Polymers," *Journal of Chemical Physics,* vol. 21, no. 7, p. 1272, 1953.

[9] A. Alexander-Katz, "Shear-Flow-Induced Unfolding of Polymeric Globules," *Physical Review Letters,* vol. 98, no. 13, 2006.

[10] N. Hoda., R.G. Larson, "Brownian dynamics simulations of single polymer chains with and without self-entanglements in theta and good solvents under imposed flow fields," *AIP Scitation Society of Rheology,* vol. 54, no. 5, pp. 1061-1081, 2010.

[11] H. KUHN, Principles of Physical Chemistry, 2nd Edition, Wiley, 2009.

[12] R. G. Larson, "The rheology of dilute solutions of flexible polymers: Progress and problems," *Journal of Rheology* , vol. 49, no. 1, pp. 1-70, 2005.

[13] P. R. Sundararajan, "Theta temperatures," in Physical Properties of Polymers Handbook, New York: AIP Press, 1996, pp. 259-287.

[14] P. S. Doyle, "BROWNIAN DYNAMICS SIMULATIONS OF POLYMERS AND SOFT MATTER," MIT, Boston, 2005.

[15] J. F. Marko, E.D. Siggia, "Stretching DNA," *Macromolecules,* vol. 28, pp. 8759-8770, 1995.

[16] P.T. Underhill, P. S. Doyle, "On the coarse-graining of polymers into bead-springchains," *Journal of Non-Newtonian Fluid Mechanics,* vol. 122, no. 1-3, pp. 3-31, 2004.

[17] P. Grassia, E.J. Hinch, "Computer simulations of polymer chain relaxation via Brownian motion," *Journal of Fluid Mechanics,* vol. 308, pp. 255-288, 1996.

[18] D. Ermak, "Brownian dynamics with hydrodynamic interactions," *AIP Journals,* vol. 69, no. 4, pp. 1352-1361, 1978.

[19] P. Szymczak, M. Cieplak, "Hydrodynamic effects in proteins," *JOURNAL OF PHYSICS: CONDENSED MATTER,* vol. 23, 2011.

[20] C. Oseen, Hydrodynamik, Leipzig, 1928.

[21] J. M. Burgers, Second report on viscosity and plasticity, Academy of Sciences, Amsterdam, 1938.

[22] J. Rotne, S. Prager, "Variational treatment of hydrodynamic," *The Journal of chemical physics,* vol. 50, no. 11, pp. 4831-4837, 1969.

[23] S. Kumar, R.G. Larson, "Brownian dynamics simulations of flexible polymers with spring-spring repulsions," *Journal of Chemical Physics,* vol. 114, pp. 6937-6941, 2001.

[24] P. Szymczak, M. Cieplak, "Proteins in a shear flow," *JOURNAL OF CHEMICAL PHYSICS,* vol. 127, no. 15, p. 155106, 2007.

[25] S. W. Schneider, "Shear-induced unfolding triggers adhesion of von Willebrand factor fibers," *PNAS,* vol. 104, pp. 7899-7903, 2007.

[26] M. Doi, S. F. Edwards, The Theory of Polymer Dynamics, New York: Clarendon Press, Oxford, 1986.

Vita

Wei Wei was born in Shanghai, China on 8 June, 1985, the son of Luguang Wei and Ling Liang. After completing his work at Shanghai Weiyu High School, he went on to Shanghai Jiao Tong University, Shanghai, China, where he received his Bachelor's degree in Mechanical Engineering in May 2007. Afterwards he entered The Graduate School at Lehigh University, USA, to pursue his Master of Science degree. He also participated in the Lehigh University's Industrial Assessment Center program.